Oxygen nonstoichiometry and defect equilibrium in electron doped $Ca_{0.6-y}Sr_{0.4}La_yMnO_{3-\delta}$

ARTICLE *in* JOURNAL OF ALLOYS AND COMPOUNDS · JULY 2015

Impact Factor: 3 · DOI: 10.1016/j.jallcom.2015.03.048

6 AUTHORS, INCLUDING:

Ekaterina I. Goldyreva
Russian Academy of Sciences
8 PUBLICATIONS **47** CITATIONS
SEE PROFILE

Ivan I. Leonidov
Russian Academy of Sciences
24 PUBLICATIONS **71** CITATIONS
SEE PROFILE

V. L. Kozhevnikov
Russian Academy of Sciences
168 PUBLICATIONS **1,841** CITATIONS
SEE PROFILE

Journal of Alloys and Compounds 638 (2015) 44–49

Contents lists available at ScienceDirect

Journal of Alloys and Compounds

journal homepage: www.elsevier.com/locate/jalcom

Oxygen nonstoichiometry and defect equilibrium in electron doped $Ca_{0.6-y}Sr_{0.4}La_yMnO_{3-\delta}$

Ekaterina I. Goldyreva [a], Ilia A. Leonidov [a,*], Mikhail V. Patrakeev [a], Andrey V. Chukin [b], Ivan I. Leonidov [a], Victor L. Kozhevnikov [a]

[a] Institute of Solid State Chemistry, Ural Branch, Russian Academy of Sciences, 620990 Ekaterinburg, Russian Federation
[b] Ural Federal University, 620002 Ekaterinburg, Russian Federation

ARTICLE INFO

Article history:
Received 11 December 2014
Received in revised form 19 February 2015
Accepted 6 March 2015
Available online 16 March 2015

Keywords:
Perovskite type oxides
$CaMnO_3$
Electron doped manganites
Oxygen nonstoichiometry
Defects chemistry
Electron transport

ABSTRACT

The perovskite-like electron doped manganites $Ca_{0.6-y}Sr_{0.4}La_yMnO_{3-\delta}$ ($0 \leqslant y \leqslant 0.15$) were synthesized in order to study oxygen content variations with composition, temperature and oxygen partial pressure. The samples are characterized with orthorhombic *Pnma* structure at $0 < y < 0.1$ and tetragonal *I* 4/*mcm* structure at $y \geqslant 0.13$ according to room temperature powder X-ray diffraction (XRD). The high-temperature data of XRD in air show transition to cubic $Pm\bar{3}m$ structure at heating above 550 °C. The variations of oxygen content in $Ca_{0.6-y}Sr_{0.4}La_yMnO_{3-\delta}$ with temperature and oxygen pressure were measured using thermogravimetry and coulometric titration at temperatures between 650 and 950 °C in the oxygen pressure range 10^{-4}–0.7 atm. The oxygen nonstoichiometry δ changes in $Ca_{0.6-y}Sr_{0.4}La_yMnO_{3-\delta}$ are observed to considerably decrease with the increase in lanthanum content. In order to explain the nonstoichiometry data, a thermodynamic model is developed based on defect formation reactions $2Mn^{3+} + V_O + ½O_2 = 2Mn^{4+} + O^{2-}$ and $2Mn^{4+} = Mn^{3+} + Mn^{5+}$. The respective equilibrium constants, defect formation enthalpies and entropies are obtained. The concentrations of different defects are calculated as functions of temperature, oxygen pressure and lanthanum content. The high-temperature conductivity measurements are carried out for independent verification of the suggested model.

1. Introduction

Electron-doped manganites $A_{1-x}Ln_xMnO_{3-\delta}$ and $AMn_{1-x}B_xO_{3-\delta}$ (A = Ca^{2+}, Sr^{2+}, Ln^{3+}, Bi^{3+}, Ce^{4+} and B = V^{5+}, Nb^{5+}, Ta^{5+}, Mo^{6+}, W^{6+}) maintain invariable perovskite-like structure in wide temperature limits, and exhibit simultaneously large values of Seebeck coefficient (S) and electrical conductivity (σ) on the background of small heat conductivity (κ) thus giving promise as materials for *n*-type legs of high temperature air-operated thermoelectric converters [1–14]. The dimensionless figure-of-merit, $ZT = S^2\sigma T/\kappa$, in $Ca_{1-x}Sr_xMn_{1-y}Mo_yO_{3-\delta}$ has been recently shown to increase considerably at partial replacement of Ca^{2+} for Sr^{2+} cations [15]. Since the highest ZT in manganites is achieved at temperatures about 1200 K [12,16], it is important to understand how oxygen nonstoichiometry changes influence their electric and heat transport parameters [17,18].

Manganites based on $CaMnO_{3-\delta}$ have attracted also a great attention recently as oxygen carriers for combustion processes due to their ability of taking up and releasing gas-phase oxygen at conditions relevant for generation of heat and power [19–27]. Therefore, exact knowledge of oxygen nonstoichiometry variations with altering factors in the surroundings such as temperature, pressure or activity of oxygen is important for development of practical applications. The iso- or heterovalent doping, e.g. substitution of Ca^{2+} for Sr^{2+} and La^{3+} cations, has a considerable impact on the capability of the manganite to exchange crystal lattice oxygen with the ambient gas phase. Thus, strontium doping is accompanied by increase of oxygen content range where δ can vary [28], which is favorable for using of the material as an oxygen carrier. On the contrary, lanthanum doping results in smaller variations of δ with environmental conditions [29], and in better stability and higher reactivity with CH_4 [26]. Generally, there is a promise that solid solutions $Ca_{1-x-y}Sr_xLa_yMnO_{3-\delta}$ can be applied at elevated temperatures as thermoelectrics and oxygen carriers. However, the mechanisms underlying nonstoichiometry variations and related functional properties in electron doped derivatives of $CaMnO_{3-\delta}$ still remain unclear.

According to [30,31] the strontium solubility limit in $Ca_{1-x}Sr_xMnO_{3-\delta}$ at synthesis in the air is close to $x = 0.45$. Similarly to the parent manganite $CaMnO_{3-\delta}$, these solid solutions maintain orthorhombic perovskite-like structure at room

* Corresponding author.
E-mail address: leonidov@imp.uran.ru (I.A. Leonidov).

http://dx.doi.org/10.1016/j.jallcom.2015.03.048
0925-8388/

temperature. The temperature increase results in step-transitions of orthorhombic–tetragonal and tetragonal–cubic structures [30,32]. The phase transition temperatures tend to decrease with the increase in strontium content. In order to obtain electron doped derivatives of $Ca_{1-x-y}Sr_xLa_yMnO_{3-\delta}$, we have chosen $Ca_{0.6}Sr_{0.4}MnO_{3-\delta}$ as a basic material where the range of homogeneous oxygen content is particularly large [28]. The lanthanum content can be raised to $y \approx 0.3$ in the $Ca_{0.6-y}Sr_{0.4}La_yMnO_{3-\delta}$ manganites [31]. Substitution of Ca^{2+} for La^{3+} cations allows varying the oxygen nonstoichiometry and independent affect the Mn^{3+} concentration at small values of δ.

In order to elucidate the reactions that govern oxygen disordering in $CaMnO_{3-\delta}$ based manganites, we have synthesized a series of samples $Ca_{1-x-y}Sr_xLa_yMnO_{3-\delta}$ ($x = 0.4$, $0 \leqslant y \leqslant 0.15$) and carried out measurements of nonstoichiometry changes at variations of temperature and oxygen partial pressure. The obtained data have been utilized for development of a defect equilibrium model.

2. Experimental

The samples $Ca_{1-x-y}Sr_xLa_yMnO_{3-\delta}$ ($x = 0.4$ and $y = 0$, 0.03, 0.05, 0.07, 0.10, 0.13, 0.15) were synthesized via glycine–nitrate process [33]. The starting reagents $CaCO_3$ (99.6%), $SrCO_3$ (99.9%), La_2O_3 (99.9%) and Mn_2O_3 (99.0%) were weighed in appropriate amounts and placed in a quartz glass where nitric acid was then added till their complete dissolution. After this the amino-acetic acid was added to form a homogeneous viscous gel. The gradual heating resulted in desiccation followed by ignition and burning of the gel. The obtained fine black powder was pressed under uni-axial load of 2 kBar into pellets of 2 mm thickness and 12 mm diameter. The pellets were fired in air at 900 °C for two hours, cooled down, crushed and repelletized. Then the temperature was raised to 1320 °C where calcination continued for 10 h, after which the samples were cooled down to room temperature with the rate of about 1 °C/min.

The obtained specimens were analyzed by powder X-ray diffraction (XRD) at room temperature using a Shimadzu XRD-7000 diffractometer with Cu $K\alpha$-radiation. The synthesized materials were scanned within $10° \leqslant 2\theta \leqslant 90°$ to confirm single-phase purity of the samples (Fig. 1). X-ray diffraction patterns at high temperatures were collected in the 2θ range 20–92° on an XPert PRO MPD diffractometer with Cu $K\alpha$-radiation. A high-temperature Anton Paar HTK 1200N camera was employed for heating. The heating rate was 20°/min. The samples were equilibrated for 10 min at desired temperature prior to data collection. The lattice parameters and volume of $Ca_{1-x-y}Sr_xLa_yMnO_{3-\delta}$ were determined from the XRD data using the PowderCell 2.3 calculation package [34].

The electrical four-probe d.c. conductivity measurements were carried out using the rectangular bars cut from the sample pellets sintered in air. The electrical parameters of the experiment were measured by high-precise voltmeter Solartron 7081.

The nonstoichiometry (δ) and total oxygen content ($3-\delta$) changes at heating in the air ($p_{O_2} = 0.21$ atm) were measured using a Setaram Setsys Evolution-1750 thermoanalyzer under assumption [15,28] that the starting oxygen content in the as-prepared samples was $(3-\delta) = 3.0$. The nonstoichiometry variations in $Ca_{0.6-y}Sr_{0.4}La_yMnO_{3-\delta}$ ($y = 0$, 0.05 and 0.15) were also measured as a function of oxygen partial pressure at different temperatures by means of the coulometric titration technique based on oxygen sensing and pumping properties of zirconia solid electrolytes [35]. The measuring cell with the volume of 0.45 cm^3 was made of cubically stabilized zirconia (YSZ), and equipped with two platinum electrodes that served as oxygen pressure sensor and/or pump. The finely milled manganite powder with the mass of about 200 mg (the error of weighing ± 0.01 mg) was placed in an alumina liner and set in the cell. The cell was covered with a YSZ lid. The space in between the lid and the cell was filled with high-temperature glass–ceramic sealant. Then the equipped measuring cell was set upon the holder and covered with the auxiliary YSZ tube with a closed butt end. The auxiliary covering tube was supplied with two pairs of platinum electrodes that served independently as oxygen pump and sensor. The covering tube was gas tightened with flanges and rubber rings at the cold end while the part around the measuring cell and pumping/sensing electrodes could have been heated with an external furnace. The assembly of the covering auxiliary cell with the measuring cell inside was evacuated with the help of a backing pump and filled with 90% O_2:10% CO_2 gas mixture prior to measurements. The experiment started from the heating of the assembly up to 1070 °C. The softening of the glass–ceramic sealant in between the lid and the cell resulted in partition of the spaces inside and outside the cell. The heating temperature was decreased to 950 °C after completion of the sealing procedure. The titration was carried out by incremental extraction of oxygen from the enclosed volume in the measuring cell. The current through the electrochemical pump of the auxiliary covering cell was maintained in a special regime so that the oxygen pressure over the measuring cell was always close to the oxygen pressure inside it. This mode of operation resulted in minimization of oxygen leaks inside the measuring cell through its' walls owing to a small electron conductivity of the solid electrolyte YSZ.

The partial pressure of oxygen (p_{O_2}) inside the measuring cell was calculated from the known expression

$$\ln p_{O_2} = \exp\left((E_m + E_c)\frac{4F}{RT}\right) + \ln p_{O_2}^{ref}, \quad (1)$$

where E_m and E_c denote potential difference at electrodes of the measuring and covering cell, respectively, F is the Faraday constant, R is the gas constant, T is absolute temperature and $p_{O_2}^{ref} = 0.21$ atm is the partial pressure of oxygen at reference electrode. The passage of oxygen ion current through the electrodes of the measuring cell resulted in the respective change of the equilibrium between the sample and gas phase oxygen followed by gradual relaxation of oxygen pressure inside the cell owing to the capacity of the manganite to take in or release oxygen. The new equilibrium was considered to be attained when condition $d(\log(p_{O_2}/\text{atm}))/dt < 0.01\ h^{-1}$ had been satisfied. Then the measured change of equilibrium pressure was used in order to calculate respective change of oxygen content in the manganite. This routine was carried out at 950 °C till the desired low pressure limit of the experiment was achieved. Similar backward steps with gradual increase of oxygen partial pressure inside the measuring cell were performed in order to confirm reproducibility of the experimental data and reversibility of the entire titration isotherm. When the upper limit of oxygen partial pressure in the measuring cell was achieved the temperature was gradually decreased to 900 °C. The respective change of the equilibrium oxygen pressure over the sample was calculated from (1), and titration procedure was repeated at 900 °C and further on down to 650 °C with the temperature step of 50 °C.

The electric parameters were measured with the help of a Solartron 7081 voltmeter. The oxygen pumps were supplied by programmable d.c. sources Yokogawa 7651. The temperature control accuracy ±1 °C was maintained using a Yokogawa UT155 controller. The setting of experimental parameters and data collection were carried out with the help of a computer. The oxygen content in $Ca_{0.6-y}Sr_{0.4}La_yMnO_{3-\delta}$ at 700 °C as determined by TG measurements in air conditions was selected as a reference point for the coulometric titration data. The uncertainty in the obtained δ values did not exceed ±0.002.

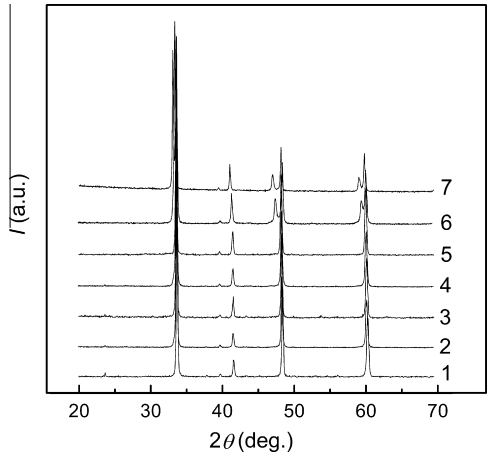

Fig. 1. Room temperature powder X-ray diffraction data for $Ca_{0.6-y}Sr_{0.4}La_yMnO_{3-\delta}$ at $y = 0$ (1), 0.03 (2), 0.05 (3), 0.07 (4), 0.10 (5), 0.13 (6) and 0.15 (7).

3. Results and discussion

3.1. Structural features

Powder XRD patterns of as-synthesized $Ca_{0.6-y}Sr_{0.4}La_yMnO_{3-\delta}$ show formation of single-phase perovskite-like samples, Fig. 1. The specimens $0 < y < 0.1$ are orthorhombic (S.G. *Pnma*) at room temperature, while tetragonal structure (S.G. *I* 4/*mcm*) is observed at $y \geqslant 0.13$. The structural parameters for the manganite with $y = 0$ coincide closely with the earlier data for $Ca_{0.6}Sr_{0.4}MnO_{3-\delta}$ [30]. A gradual increase of the unit cell volume of $Ca_{0.6-y}Sr_{0.4}La_yMnO_{3-\delta}$ is consistent with the increase in concentration of large charge-compensating Mn^{3+} cations that appear in response to lanthanum doping (Fig. 2). However, the lattice parameters change abruptly near $y = 0.12$. This behavior reflects elongation of MnO_6 octahedra along *c*-axis due to Jahn–Teller distortions, which indicate

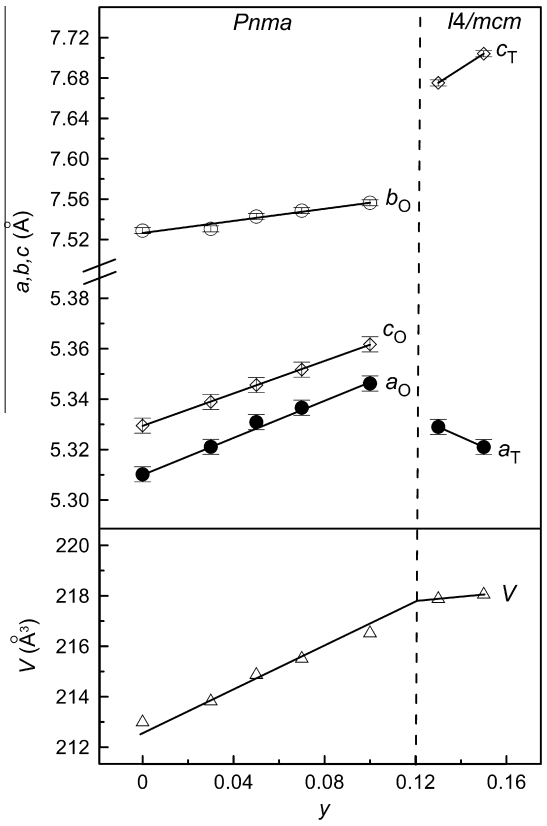

Fig. 2. The lattice parameters in $Ca_{0.6-y}Sr_{0.4}La_yMnO_{3-\delta}$ at different lanthanum content.

themselves as a collective phenomenon at sufficiently large concentration of Mn^{3+} cations [36,37].

3.2. Oxygen nonstoichiometry

The oxygen content changes in $Ca_{0.6-y}Sr_{0.4}La_yMnO_{3-\delta}$ at heating in the air are shown in Fig. 3. Oxygen depletion from undoped $Ca_{0.6}Sr_{0.4}MnO_{3-\delta}$ arises at about 400 °C. Meanwhile, lanthanum incorporation in the alkaline-earth metal sub-lattice, even a small one, results in an increase of the oxygen release temperature that approaches about 600 °C for $Ca_{0.55}Sr_{0.4}La_{0.05}MnO_{3-\delta}$. Moreover, the concentration growth of the donor La^{3+} centers favors a considerable decrease in the overall changes of oxygen content. This effect can be related with the respective increase in the reduction enthalpy ΔH°_{Red} that governs formation of oxygen vacancies V_O and Mn^{3+} cations

$$2Mn^{4+} + O^{2-} = V_O + 2Mn^{3+} + \frac{1}{2}O_2 + \Delta H^{\circ}_{Red}, \quad (2)$$

so that the removal of the equal amount of oxygen from the crystal lattice takes stronger heating for $Ca_{0.6-y}Sr_{0.4}La_yMnO_{3-\delta}$ in comparison with $Ca_{0.6}Sr_{0.4}MnO_{3-\delta}$. In writing (2) and other reactions below we use nominal charges for the involved species. The relations with quasi-chemical notations are $Mn^{3+} \equiv Mn'_{Mn}$, $Mn^{4+} \equiv Mn^{\times}_{Mn}$, $Mn^{5+} \equiv Mn^{\cdot}_{Mn}$, $O^{2-} \equiv O^{\times}_{O}$ and $V_O \equiv V^{\cdot\cdot}_{O}$.

The isothermal plots of total oxygen content changes in $Ca_{0.6-y}Sr_{0.4}La_yMnO_{3-\delta}$ at variations of $\log p_{O_2}$ exhibit rather ample oxygen loss at oxygen pressure decrease within 650–950 °C, Figs. 4–6. The reversible changes of δ may achieve 0.20–0.24 at 950 °C and $p_{O_2} = 10^{-4}$ atm. These values are typical for extreme oxygen nonstoichiometry in $Ca_{1-x}Sr_xMnO_{3-\delta}$ [38]. Moreover, a smooth shape of $(3-\delta)$ vs. $\log p_{O_2}$ plots shows that oxygen intake and release in $Ca_{0.6-y}Sr_{0.4}La_yMnO_{3-\delta}$ is not accompanied with structural changes unlike to $CaMnO_{3-\delta}$ [39]. This conclusion is corroborated with high-temperature XRD results that evidence invariably cubic structure (S.G. $Pm\bar{3}m$) of $Ca_{0.6-y}Sr_{0.4}La_yMnO_{3-\delta}$ at temperatures above 550 °C (Fig. 7). The obtained equilibrium $p_{O_2} - T - \delta$ diagrams (Figs. 4–6) can be employed to calculate the defect concentrations and respective equilibrium constants that govern defect formation in $Ca_{0.6-y}Sr_{0.4}La_yMnO_{3-\delta}$.

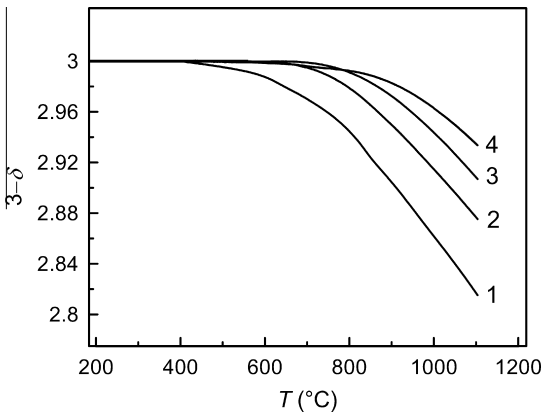

Fig. 3. Oxygen content variations in $Ca_{0.6-y}Sr_{0.4}La_yMnO_{3-\delta}$, $y = 0$ (1), 0.05 (2), 0.10 (3) and 0.15, at heating in the air with the rate of 10 °/min.

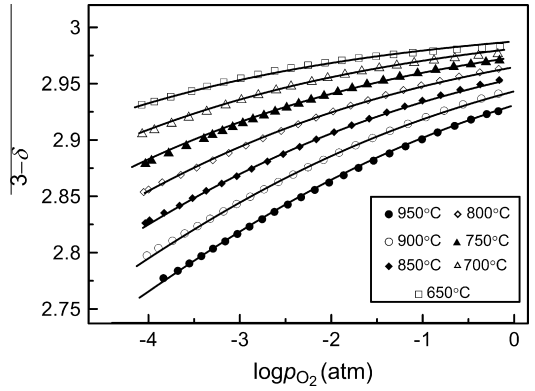

Fig. 4. Isothermal changes of oxygen content in $Ca_{0.6}Sr_{0.4}MnO_{3-\delta}$ at variations of oxygen partial pressure. Solid lines show best fitting results according to Eq. (12).

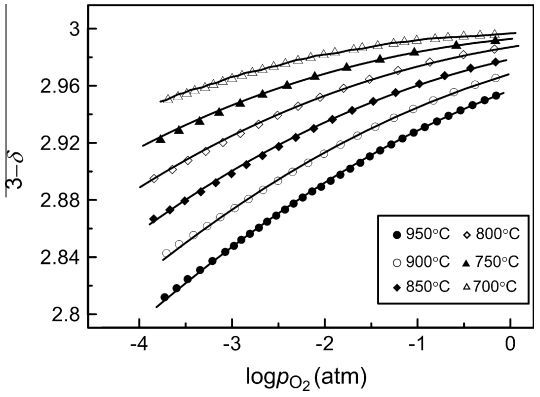

Fig. 5. Isothermal changes of oxygen content in $Ca_{0.6-y}Sr_{0.4}La_yMnO_{3-\delta}$ ($y = 0.05$) at variations of oxygen partial pressure. Solid lines show best fitting results according to Eq. (12).

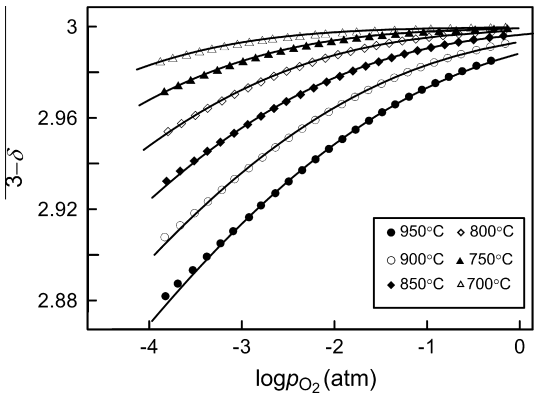

Fig. 6. Isothermal changes of oxygen content in $Ca_{0.6-y}Sr_{0.4}La_yMnO_{3-\delta}$ ($y = 0.15$) at variations of oxygen partial pressure. Solid lines show best fitting results according to Eq. (12).

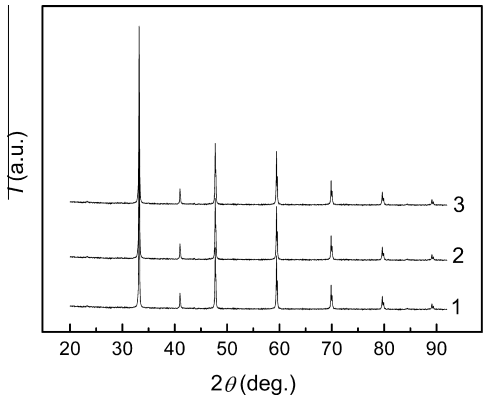

Fig. 7. Powder X-ray diffraction data for $Ca_{0.6-y}Sr_{0.4}La_yMnO_{3-\delta}$ at 550 °C; $y = 0.03$ (1), 0.07 (2), 0.15 (3).

3.3. Defect equilibrium

The electron structure calculations [40] show that the forbidden energy gap E_g is about 0.46 and 0.30 eV in cubic $CaMnO_{3-\delta}$ and $SrMnO_{3-\delta}$, respectively. Assuming that E_g in $Ca_{0.6}Sr_{0.4}MnO_{3-\delta}$ is in between these values one can estimate the n concentration of intrinsic electrons (i.e. Mn^{3+} cations) that appear at thermal excitation of Mn^{4+} cations

$$2Mn^{4+} = Mn^{3+} + Mn^{5+}. \quad (3)$$

In order to do so we can use the known expression $n = \sqrt{N_C N_V}\exp(-E_g/2kT)$ [41], where $N_C \sim 1$ and $N_V \sim 1$ stand for the effective density of states per unit cell in conduction and valence bands, respectively, and E_g is taken to be about 0.4 eV. Simple calculations show that $n \sim 0.1$ at 1000 K. On the other hand, oxygen loss at heating

$$Ca_{0.6}Sr_{0.4}MnO_3 = Ca_{0.6}Sr_{0.4}MnO_{3-\delta} + \delta/2O_2, \quad (4)$$

results in appearance of $n = 2\delta$ electrons. Typical δ values in $Ca_{0.6}Sr_{0.4}MnO_{3-\delta}$ may vary within 0.03–0.10 at temperatures near 1000 K as one can see in Fig. 3. The corresponding changes in electron concentration can consequently achieve 0.06–0.20, which is comparable with the amount of thermally exited intrinsic electrons. Therefore, thermal excitation and oxygen exchange reactions are both to be taken into account in defect structure analysis.

Oxidation of Mn^{3+} cations in $Ca_{0.6-y}Sr_{0.4}La_yMnO_{3-\delta}$ can be expressed as:

$$2Mn^{3+} + V_O + \frac{1}{2}O_2 = 2Mn^{4+} + O^{2-} + \Delta H^\circ_{Ox}. \quad (5)$$

The equilibrium constants K_D and K_{Ox} for reactions (3) and (5), respectively, can be represented as:

$$K_D = \frac{[Mn^{3+}][Mn^{5+}]}{[Mn^{4+}]^2} \quad K_{Ox} = \frac{[O^{2-}][Mn^{4+}]^2}{p_{O_2}^{1/2}[V_O][Mn^{3+}]^2}. \quad (6)$$

Introducing concentrations of manganese cations according to crystallochemical formula $Ca_{0.6-y}Sr_{0.4}La_yMn_g^{4+}Mn_n^{3+}Mn_p^{5+}O_{3-\delta}$, one can write the structure conservation and charge neutrality requirements as:

$$g + n + p = 1, \quad (7)$$

$$n = p + 2\delta + y. \quad (8)$$

Combining these equalities with K_D

$$K_D = \frac{n \cdot p}{g^2}, \quad (8)$$

one can obtain

$$p = \frac{4K_D - 8\delta K_D + 2\delta - 4yK_D + y - D}{8K_D - 2}, \quad (9)$$

$$n = 2\delta + y + \frac{4K_D - 8\delta K_D + 2\delta - 4yK_D + y - D}{8K_D - 2}, \quad (10)$$

$$g = 1 - 2\delta - y - \frac{4K_D - 8\delta K_D + 2\delta - 4yK_D + y - D}{4K_D - 1}, \quad (11)$$

where $D = \sqrt{4K_D - 16\delta y K_D + 4\delta y + y^2 + 4\delta^2 - 4y^2K_D - 16\delta^2 K_D}$

Then, expressions (10) and (11) can be substituted in K_{Ox} (6) in order to derive interrelation between δ and p_{O_2}

$$p_{O_2}^{1/2} = \frac{1}{K_{Ox}}\frac{(3-\delta)}{\delta}\frac{g^2}{n^2}. \quad (12)$$

This equation can be used together with (10) and (11) to simulate experimental isotherms in Figs. 4–6 by selecting appropriate values for K_D and K_{Ox}. The respective fitting results in numerical values of the K_D and K_{Ox} constants at different temperatures. Comparison of the experimental data with the calculated results in Figs. 4–6 demonstrates good quality of the fitting and reliability of the utilized defect model.

The Arrhenius plots for K_D and K_{Ox} in Fig. 8 provide a straightforward means to determine the standard enthalpies ΔH° and entropies ΔS° for reactions (3) and (5) according to the known thermodynamic relation

$$-RT\ln K = \Delta G^\circ = \Delta H^\circ - T\Delta S^\circ. \quad (13)$$

The linear least square fitting procedures result in ΔH°_{Ox}, ΔH°_D and ΔS°_{Ox}, ΔS°_D, Table 1. The lanthanum doping is accompanied with the increase in absolute values for ΔH°_{Ox} and ΔH°_D. The ΔH°_{Ox} growth is consistent with TG data in Fig. 3 and provides a natural explanation to the observed decrease of δ with the increase of lanthanum content in $Ca_{0.6-y}Sr_{0.4}La_yMnO_{3-\delta}$. The obtained enthalpy ΔH°_D in $Ca_{0.6-y}Sr_{0.4}La_yMnO_{3-\delta}$ varies from 28.8 kJ/mol at $y = 0$–41.6 kJ/mol at $y = 0.15$, which appears to be in a reasonable accord with the forbidden gap 29.0 kJ/mol in $SrMnO_{3-\delta}$ and 44.4 kJ/mol in $CaMnO_{3-\delta}$ [40].

Eqs. 9–12 can be used in order to calculate concentration of manganese cations and oxygen vacancies at different values of oxygen pressure, temperature and lanthanum content. Respective plots are shown in Figs. 9–11. It is seen that at moderate temperatures, 650–700 °C, n- and p-type defects (Mn^{3+} and Mn^{5+} cations) in $Ca_{0.6}Sr_{0.4}MnO_{3-\delta}$ become dominant at elevated pressures,

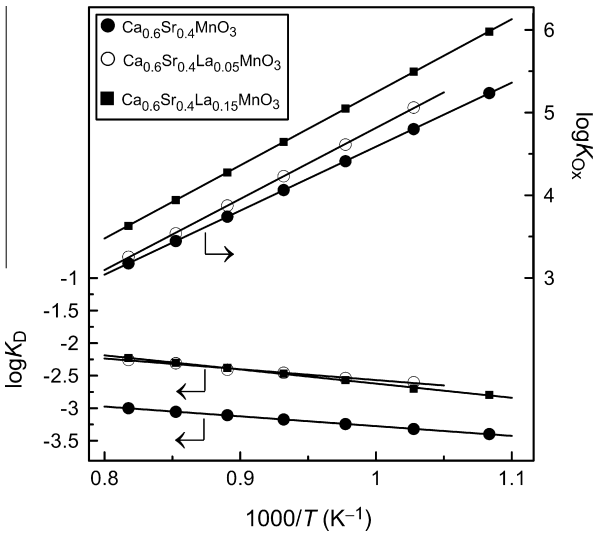

Fig. 8. Logarithmic dependencies of equilibrium constants on inverse temperature for cubic $Ca_{0.6-y}Sr_{0.4}La_yMnO_{3-\delta}$.

Table 1
The enthalpy and entropy values for reactions (3) and (5) in cubic $Ca_{0.6-y}Sr_{0.4}La_yMnO_{3-\delta}$.

y	ΔH°_{Ox} (kJ mol^{-1})	ΔS°_{Ox} (J mol^{-1} K^{-1})	ΔH°_D (kJ mol^{-1})	ΔS°_D (kJ mol^{-1} K^{-1})
0	−148.2	−60.4	28.8	−33.9
0.05	−164.6	−72.4	31.7	−17.4
0.15	−169.3	−68.9	41.6	−8.6

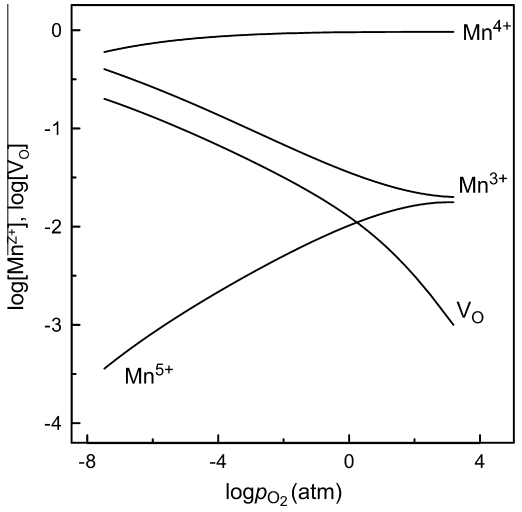

Fig. 9. Calculated logarithmic plots for concentration of defect species in $Ca_{0.6}Sr_{0.4}MnO_{3-\delta}$ at variations of oxygen partial pressure and 650 °C.

$p_{O_2} > 10$ atm. Meanwhile, the concentration of Mn^{3+} cations at relatively low pressures, $p_{O_2} < 1$ atm, mainly depends on δ, Fig. 9. On the other hand, incorporation of even a small amount of lanthanum leads to a more "rigid" crystal lattice so that the Mn^{3+} concentration at moderate temperatures and elevated pressures of oxygen is mostly governed by electrical neutrality condition $n = p + y$ because oxygen nonstoichiometry variations are quite small, Fig. 10. For instance, the calculated value for δ in $Ca_{0.55}Sr_{0.4}La_{0.05}MnO_{3-\delta}$ at 700 °C in the air does not exceed 0.01, in good agreement with experimental data in Fig. 5.

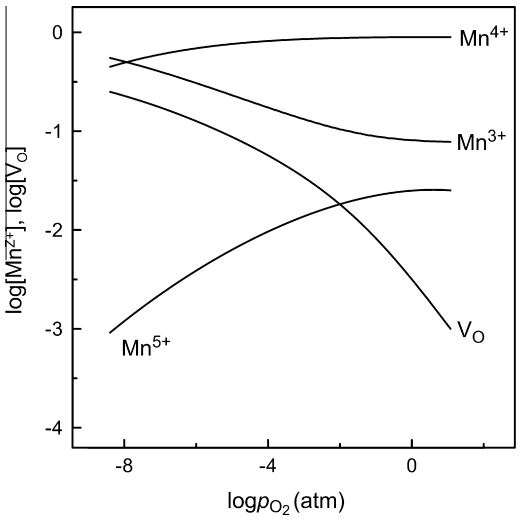

Fig. 10. Calculated logarithmic plots for concentration of defect species in $Ca_{0.6-y}Sr_{0.4}La_yMnO_{3-\delta}$ ($y = 0.05$) at variations of oxygen partial pressure and 700 °C.

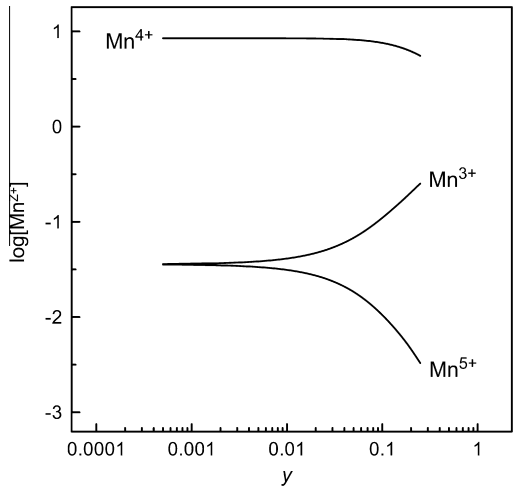

Fig. 11. Calculated changes in concentration of manganese species with lanthanum content in $Ca_{0.6-y}Sr_{0.4}La_yMnO_{3-\delta}$ at 700 °C and $\delta = 0$.

The changes in concentration of manganese cations with lanthanum content at $\delta = 0$ and $T = 700$ °C (Fig. 11) show that n-type charge carriers in lightly La-doped samples appear mostly owing to thermal excitation (3). The donor doping provides some influence upon concentration of electrons only when $y > 0.03$. At lower temperatures where δ in $Ca_{0.6-y}Sr_{0.4}La_yMnO_{3-\delta}$ is always close to zero even at wide variations of oxygen pressure, concentrations of intrinsic and extrinsic n-type charge carries are nearly equal at $y \sim 0.03$.

An independent verification of the suggested defect model can be obtained from the analysis of high-temperature electrical conductivity. The conductivity plot vs. lanthanum content in $Ca_{0.6-y}Sr_{0.4}La_yMnO_{3-\delta}$ at 500 °C is represented in Fig. 12. Assuming small polaron conduction mechanism, which usually is operative in transition metal oxides, the concentration dependent conductivity in $Ca_{0.6-y}Sr_{0.4}La_yMnO_{3-\delta}$ is expected to change as a product of charge carrier concentration [Mn^{3+}] and amount of positions [Mn^{4+}] available for jumps of polarons [42]. Fig. 11 shows that [Mn^{4+}] is practically independent on lanthanum content within studied doping limits. However, [Mn^{3+}] tends to increase with y in a parabolic-like manner, and so should the product $\sigma \sim [Mn^{3+}][Mn^{4+}]$. Indeed, the data in Figs. 11 and 12 confirm the

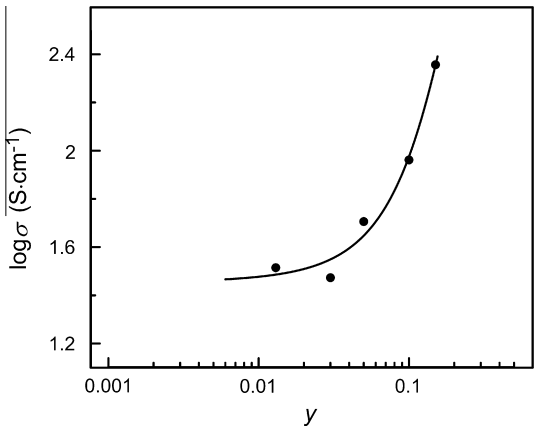

Fig. 12. Experimental data for electron conductivity at different lanthanum content in $Ca_{0.6-y}Sr_{0.4}La_yMnO_{3-\delta}$ at 500 °C in the air. The solid line is for eye guidance.

remarkable similarity of doping induced changes in calculated values of $[Mn^{3+}]$ and experimentally measured conductivity.

The calculated data for $[Mn^{3+}]$ in Fig. 11 and measured conductivity σ in Fig. 12 can be employed to evaluate mobility of electrons in $Ca_{0.6-y}Sr_{0.4}La_yMnO_{3-\delta}$ according to the known expression

$$\mu = \frac{\sigma}{e \cdot n \cdot N}, \quad (14)$$

here e is the elementary charge and N is the number of formula units per unit volume, which can be calculated from structural data in Fig. 2. The estimates show that electron mobility in $Ca_{0.6-y}Sr_{0.4}La_yMnO_{3-\delta}$ at 500 °C just slightly depends on doping and varies within 0.2–0.5 $cm^2\ V^{-1}\ s^{-1}$. These values are of the same magnitude order as the characteristic threshold 0.1 $cm^2\ V^{-1}\ s^{-1}$ separating small polaron and band conduction [43], and, therefore, do not contradict the assumed small polaron conductivity in $Ca_{0.6-y}Sr_{0.4}La_yMnO_{3-\delta}$.

4. Conclusions

The equilibrium oxygen content changes at 650–950 °C have been studied in $Ca_{0.6-y}Sr_{0.4}La_yMnO_{3-\delta}$ ($0 \leqslant y \leqslant 0.15$) within the oxygen pressure range 10^{-4}–0.7 atm. The results have been explained on the basis of the defect model that includes red/ox equilibrium Mn^{3+}/Mn^{4+} and thermal excitation of Mn^{4+} cations. The non-linear fittings of the experimental $(3-\delta)$ vs. $\log p_{O_2}$ curves with the model equations have been used in order to determine the respective equilibrium constants and changes in enthalpy and entropy with the doping level. The enthalpy values derived from thermodynamic modelling are in a reasonable agreement with the forbidden energy gap from *ab initio* calculations for similar calcium and strontium manganites. The changes in concentration of manganese species have been calculated using the obtained equilibrium constants. The calculation results are corroborated with the independent data from high-temperature electrical conductivity measurements.

Acknowledgments

Authors are grateful to the RSF for support of this work under Grant No. 14–13–00870.

References

[1] M. Ohtaki, H. Koga, T. Tokunaga, K. Eguchi, H. Arai, J. Solid State Chem. 105 (1995) 105–111.
[2] J. Hejtmánek, Z. Jirák, M. Maryško, C. Martin, A. Maignan, M. Harvieu, B. Raveau, Phys. Rev. B 60 (1999) 14057–14065.
[3] J.L. Cohn, C. Chiorescu, J.J. Neumeier, Phys. Rev. B 72 (2005) 024422.
[4] Y. Wang, Y. Sui, X. Wang, W. Su, J. Phys. D: Appl. Phys. 42 (2009) 055010.
[5] E.N. Caspi, M. Avdeev, S. Short, J.D. Jorgensen, M.V. Lobanov, Z. Zeng, M. Greenblatt, P. Thiyagarajan, C.E. Botez, P.W. Stephens, Phys. Rev. B 69 (2004) 104402.
[6] M.E. Melo Jorge, M.R. Nunes, R. Silva Maria, D. Sousa, Chem. Mater. 17 (2005) 2069–2075.
[7] R. Ang, Y.P. Sun, Y.Q. Ma, B.C. Zhao, X.B. Zhu, W.H. Song, J. Appl. Phys. 100 (2006) 063902.
[8] L. Bocher, M.H. Aguirre, D. Logvinovich, A. Shkabko, R. Robert, M. Trottmann, A. Weidenkaff, Inorg. Chem. 47 (2008) 8077–8085.
[9] G.J. Xu, R. Funahashi, Q.R. Pu, B. Liu, R.H. Tao, G.S. Wang, Z.J. Ding, Solid State Ionics 171 (2004) 147–151.
[10] A. Maignan, C. Martin, C. Autret, M. Harvieu, B. Raveau, J. Hejtmanek, J. Mater. Chem. 12 (2002) 1806–1811.
[11] M. Miclau, J. Hejtmánek, R. Retoux, K. Knizek, Z. Jirak, R. Frésard, A. Maignan, S. Hébert, M. Hervieu, C. Martin, Chem. Mater. 19 (2007) 4243–4251.
[12] P. Thiel, J. Eilertsen, S. Populoh, G. Saucke, M. Döbeli, A. Shkabko, L. Sagarna, L. Karvonen, A. Weidenkaff, J. Appl. Phys. 114 (2013) 243707.
[13] R. Kabir, T. Zhang, D. Wang, R. Donelson, R. Tian, T.T. Tan, S. Li, J. Mater. Sci. 49 (2014) 7522–7528.
[14] H. Taguchi, M. Sonoda, M. Nagao, J. Solid State Chem. 137 (1998) 82–86.
[15] T. Okuda, Y. Fujii, J. Appl. Phys. 108 (2010) 103702.
[16] P.X. Thao, T. Tsuji, M. Hashida, Y. Yamamura, J. Ceram. Soc. Jpn. 111 (2003) 544–547.
[17] M. Schrade, R. Kabir, S. Li, T. Norby, T.G. Finstad, J. Appl. Phys. 115 (2014) 103705.
[18] E.I. Goldyreva, I.A. Leonidov, M.V. Patrakeev, V.L. Kozhevnikov, J. Solid State Electrochem. 17 (2013) 1449–1454.
[19] M. Rydén, H. Leion, T. Mattisson, A. Lyngfelt, Appl. Energy 113 (2013) 1924–1932.
[20] P. Hallberg, D. Jing, M. Rydén, T. Mattisson, A. Lyngfelt, Energy Fuels 27 (2013) 1473–1481.
[21] M. Källén, M. Rydén, C. Dueso, T. Mattisson, A. Lyngfelt, Ind. Eng. Chem. Res. 52 (2013) 6923–6932.
[22] M. Arjmand, A. Hedayati, A.-M. Azad, H. Leion, M. Rydén, T. Mattisson, Energy Fuels 27 (2013) 4097–4107.
[23] L.F. de Diego, A. Abad, A. Cabello, P. Gayan, F. Garcia-Labiano, J. Adanez, Ind. Eng. Chem. Res. 53 (2014) 87–103.
[24] M. Rydén, A. Lyngfelt, T. Mattisson, Int. J. Greenhouse Gas Control 5 (2011) 356–366.
[25] H. Leion, Y. Larring, E. Bakken, T. Mattisson, R. Bredesen, A. Lyngfelt, Energy Fuels 23 (2009) 5276–5283.
[26] M. Arjmand, A. Hedayati, A. Abdul-Majeed, H. Leion, M. Rydén, T. Mattisson, Energy Fuels 52 (2013) 6923–6932.
[27] Q. Imtiaz, D. Hosseini, C.R. Müller, Energy Technol. 1 (2013) 633–647.
[28] B. Dabrowski, O. Chimaissem, J. Mais, S. Kolesnik, J.D. Jorgensen, S. Short, J. Solid State Chem. 170 (2003) 154–164.
[29] L. Rørmark, K. Wiik, S. Stølen, T. Grande, J. Mater. Chem. 12 (2002) 1058–1067.
[30] O. Chimaissem, B. Dabrowski, S. Kolesnik, J. Mais, D.E. Brown, R. Kruk, P. Prior, B. Pyles, J.D. Jorgensen, Phys. Rev. B 64 (2001) 134412.
[31] P. Majewski, L. Epple, F. Aldinger, J. Am. Ceram. Soc. 83 (2000) 1513–1517.
[32] Q. Zhou, B.J. Kennedy, J. Solid State Chem. 179 (2006) 3568–3574.
[33] L. Ronghui, D. Qingshan, M. Wenhui, W. Hua, Y. Bin, D. Yongnian, M. Xueju, J. Rare Earths 24 (2006) 98–103.
[34] W. Kraus, G. Nolze, PowderCell for Windows – Version 2.3 – Structure Visualisation/Manipulation, Powder Pattern Calculation and Profile Fitting, Federal Institute for Materials Research and Testing, Berlin, Germany, 1999.
[35] M.V. Patrakeev, I.A. Leonidov, V.L. Kozhevnikov, J. Solid State Electrochem. 15 (2011) 931–954.
[36] S.M. Dunaevskii, Phys. Solid State 46 (2004) 193–212.
[37] V.M. Loktev, Y.G. Pogorelov, Low Temp. Phys. 26 (2000) 171–193.
[38] J. Töpfer, U. Pippardt, I. Voigt, R. Kriegel, Solid State Sci. 6 (2004) 647–654.
[39] E.I. Goldyreva, I.A. Leonidov, M.V. Patrakeev, V.L. Kozhevnikov, J. Solid State Electrochem. 16 (2012) 1187–1191.
[40] R. Søndenå, S. Stølen, P. Ravindran, T. Grande, N.L. Grande, Phys. Rev. B 75 (2007) 184105.
[41] F.A. Kröger, The Chemistry of Imperfect Crystals, North-Holland, Wiley-Interscience, Amsterdam, New York, 1964.
[42] N. Mott, Conduction in Non-Crystalline Materials, Clarendon Press, Oxford, 1987.
[43] A.G. Bosman, H.J. Daal, Adv. Phys. 19 (1970) 1–117.